Properties of Saturn Kilometric Radiation measured within its source region

L. Lamy[1], P. Schippers[2], P. Zarka[3], B. Cecconi[3], C. Arridge[4], M.K.

Dougherty[1], P. Louarn[5], N. André[5], W.S. Kurth[2], R.L. Mutel[2], D.A.

Gurnett[2], A.J. Coates[4]

———

[1]Space and Atmospheric Physics, Blackett

Laboratory, Imperial College London,

London, UK

[2]Department of Physics and Astronomy,

University of Iowa, Iowa City, Iowa, USA

[3]Laboratoire d'Etudes et

d'Instrumentation en Astrophysique,

Observatoire de Paris, CNRS, Meudon,

France

[4]Centre d'Etude Spatiale des

Rayonnements, Université Paul Sabatier,

CNRS, Toulouse, France

[5]The Centre for Planetary Sciences at

UCL/Birkbeck, London, UK

D R A F T   January 21, 2011, 1:30am   D R A F T

On 17 October 2008, the Cassini spacecraft crossed the southern sources of Saturn kilometric radiation (SKR), while flying along high-latitude night-side magnetic field lines. In situ measurements allowed us to characterize for the first time the source region of an extra-terrestrial auroral radio emission. Using radio, magnetic field and particle observations, we show that SKR sources are surrounded by a hot tenuous plasma, in a region of upward field-aligned currents. Magnetic field lines supporting radio sources map a continuous, high-latitude and spiral-shaped auroral oval observed on the dawnside, consistent with enhanced auroral activity. Investigating the Cyclotron Maser Instability (CMI) as a mechanism responsible for SKR generation, we find that observed cutoff frequencies are consistent with radio waves amplified perpendicular to the magnetic field by hot (6 to 9 keV) resonant electrons, measured locally.

———

1. Introduction

In the past four decades, remote observations have identified intense radio emissions from auroral regions of all explored magnetized planets of the solar system [*Zarka*, 1998]. However, the source region of the terrestrial auroral kilometric radiation (AKR) has been the only one studied so far with in situ measurements. First observations from ISIS 1 (1970's), followed by extensive ones from Viking (1980's) and FAST (1990's) brought crucial constraints on the local plasma conditions and properties of emitted waves, leading to a comprehensive picture of AKR and its generation mechanism.

AKR is a cyclotron emission mainly emitted on the extraordinary (X) mode by auroral electrons, at frequencies close to the local gyrofrequency f_{ce}, between 50 and 700 kHz, in high-latitude tenuous regions (or auroral cavities). Signatures of AKR source crossings were identified in Viking dynamic spectra above 100 kHz by (i) an enhanced amplitude of the low-frequency emissions, typically reaching 10 mV.m^{-1}, and (ii) a cutoff frequency f_{cut} close to, and occasionally below, f_{ce} [*Bahnsen et al.*, 1989; *Roux et al.*, 1993]. X mode emission at $f \leq f_{ce}$ was related to predominant weakly relativistic (typically 5 keV) electrons [*Le Queau and Louarn*, 1989]. Indeed, radio sources lie in auroral cavities depleted in cold plasma (≤ 1 keV), where $f_{pe}/f_{ce} \leq 0.1$, and 5 to 10 times less dense than the surrounding medium. These cavities correspond to acceleration regions with large electric potential drops, characterized by downward (upward) beams of electrons (ions) [*Benson and Calvert*, 1979], along field lines connected to auroral arcs. The spatial extent of AKR source regions is elongated in altitude (0.5 to 3 R$_E$ according to the AKR spectrum, 1 R$_E$ = 6378 km), narrow in latitude (a few tens of km), more extended in lon-

gitude and time variable [*Hilgers et al.*, 1991]. Attributed to the wave-electron interaction named Cyclotron Maser Instability (CMI) [*Wu and Lee*, 1979], AKR is emitted quasi-perpendicularly from the local magnetic field [*Hilgers et al.*, 1992] by unstable trapped [*Louarn et al.*, 1990], or shell-type [*Ergun et al.*, 2000] electron distributions.

Saturn Kilometric Radiation (SKR) is the kronian equivalent of AKR. Remote observations by Voyager (flybys in 1980 and 1981) and Cassini (in orbit since mid-2004) have established that SKR is also mainly observed on the X mode between 3 and 1200 kHz (*i.e.* altitudes between 0.1 and 5 R_S, 1 R_S = 60268 km), consistent with CMI, along magnetic field lines globally associated with atmospheric aurorae [*Kurth et al.*, 2009]. However, in the absence of in situ measurements, the characteristics of the SKR source region, together with the nature and origin of the unstable resonant electrons responsible for its generation (or source of free energy), remained unknown.

The first crossing of the SKR source region was identified by Cassini on day 291 of 2008 near midnight Local Time (LT), at a distance of 5 R_S ($f_{ce} \sim 10$ kHz) and latitudes below $-60°$ [*Kurth et al.*, 2010]. Here, we investigate simultaneous observations of the Radio and Plasma Wave Science (RPWS) experiment, the magnetometer (MAG) and the Cassini Plasma Electron Spectrometer (CAPS) instrument (see auxiliary material for details of the specific data processing). We focus on the characteristics of the source region (section 2), the locus of local and distant radio sources (section 3), and investigate how the CMI mechanism can lead to the observed SKR frequencies (section 4). The results are compared with the terrestrial case.

2. Source region properties

RPWS, MAG and CAPS observations, for day 291 of year 2008 are displayed in Figure 1 between 0600 and 1100 UT. Figure 1a shows a dynamic spectrum of electric spectral density measured on one RPWS monopole between 3.5 and 1500 kHz. Except around 0848 and 0924 UT, where the antenna detected little signal above 100 kHz, due to its quasi-alignment with incoming wave vectors, the SKR spectrum extends from $\sim f_{ce}$ to 1000 kHz. Criteria (i) and (ii), as used to identify AKR source crossings at Earth, are clearly satisfied at low frequencies, around 10 kHz. First, (i) the low-frequency SKR amplitude particularly increases. Indeed, once calibrated, corrected for the actual distance to each source (see section 3) and normalized to 1 AU, the SKR intensity reaches $\sim 10^{-18}$ W.m^{-2}.Hz^{-1}, *i.e.* the upper 1% quantile of SKR mid-latitudes observations at 10 kHz [*Lamy et al.*, 2008]. Then, (ii) the SKR spectrum shows a cutoff around f_{ce}. Frequencies f_{cut} (see auxiliary text and Figures S1,2), as well as f_{ce}, are quantitatively investigated in Figure 1b. Whereas f_{cut} approaches f_{ce} from 0748 to 1000 UT, the amplitude is especially intense close to f_{ce} between 0812 and 0912 UT (orange shaded, hereafter called the source region), with three unambiguous excursions below f_{ce} (red shaded, labelled A, B and C). There, the SKR peaks at $\sim 10^{-9}$ V^2.Hz^{-1} within the $[f_{ce}-1\mathrm{kHz}, f_{ce}+4\mathrm{kHz}]$ bandwidth, corresponding to a field strength of ~ 1 mV.m^{-1}. Events A, B and C display negative $(f_{cut} - f_{ce})/f_{ce}$, as low as $\sim -2\%$, considered at Earth as the best indication of AKR sources, as a result of predominant hot electrons. This feature is investigated in section 4.

Frequencies f_{cut} and f_{ce} are reproduced in the logarithmic plot of Figure 1c, together with the plasma frequency f_{pe} (density) and its contributions from cold, warm, and hot

electrons, derived from CAPS measurements. The uncertainty on the above values (typically $\leq 30\%$, see auxiliary Figure S3) is mainly due to the underestimate of cold electrons masked by the spacecraft positive potential, and electrons missed by incomplete and time variable pitch angle coverage. The total density does not display any terrestrial-like cavity devoid of cold electrons (where $f \leq f_{ce}$) and surrounded by a denser and colder medium (where $f \geq f_{ce}$). Rather, we observe a large tenuous region, comprising a sporadic warm component, and dominated by hot electrons after 0700 UT, for latitudes $\lambda_{sc} \leq -50°$ and distances $4.1 \leq r_{sc} \leq 5.8$ R$_S$. Corresponding relative altitudes being much larger than at Earth, possible auroral cavities may be present closer to Saturn. Within the source region, the total electron plasma frequency f_{pe} varies between 400 and 900 Hz, leading to f_{pe}/f_{ce} ratios of 0.05-0.09, in agreement with requirements for CMI resonance and observed AKR generation conditions. Contrary to the situation at Earth, the kronian auroral plasma environment appears to be naturally tenuous/magnetized enough to generate SKR, where CMI-unstable electrons are present.

Figure 1d investigates the azimuthal component of the magnetic field. Gradients in B_ϕ indicate field-aligned currents (FAC) where the sign of the slope gives the direction (up- or downgoing) of the local net current. The source region (orange) corresponds to a positive slope starting at 0748 UT, and events A, B and C nearly match the steepest positive slopes. This trend suggests a globally upward current, associated with downward electrons, and consistent with observed upward ions [*Kurth et al.*, 2010], similar to observations within AKR sources. We also note a strong positive slope around 0630 UT, where no signature

of SKR sources was detected. This can be explained by $f_{pe}/f_{ce} \geq 0.5$ preventing CMI resonance.

MAG measurements thus complement CAPS observations shown by the electron spectrogram of Figure 1e, where the incomplete pitch angle coverage did not allow the detection of down-going electrons with pitch angles $\leq 15°$. The phase space density of detected electrons reveals two sporadic distributions: a partial shell-like distribution for 1-10 keV (hot) electrons, that displays part of the expected down-going electrons, most likely accelerated at higher altitudes, and up-going field-aligned beams of a few 100 eV (warm) electrons. Both distributions, possible candidates for SKR generation, are observed during and outside of events A, B and C. They might thus complete the criteria used to identify source regions. Finally, no loss cone was observed in the electron distributions. The predicted loss cone angle $\alpha \sim 5°$ at such altitudes, was however smaller than the CAPS angular resolution.

3. Location of SKR sources

RPWS-HFR 3-antenna observations unambiguously provide the wave vector $\mathbf{k}$ of each time-frequency measurement, assuming transverse waves and instantaneous point sources [*Cecconi and Zarka*, 2005]. Under the hypothesis of SKR generation at $f = f_{ce}$, *Cecconi et al.* [2009] used the SPV magnetic field model, and a simple current sheet, to derive the intersection of each $\mathbf{k}$ vector with the corresponding isosurface $f = f_{ce}$, giving the 3D spatial source location and its associated field line.

This remote sensing capability was used within the source region to determine the instantaneous 3D location of both local and distant radio sources. Figures 2a,b show the

spatial distribution of low-frequency SKR sources over the interval [0812,0912] UT, as observed from Cassini and after magnetic polar projection. The radio source localization technique yields more accurate locations for sources closer to the spacecraft, *i.e.* lowest frequencies. Radio emissions at $f \geq f_{ce}+1\text{kHz}$ reveal distant sources (blue) organized along dawnside high-latitude magnetic field lines, with, as expected, sources closer to the planet for increasing frequencies. Footprints of associated field lines, known to map to part of a circumpolar radio auroral oval [*Lamy et al.*, 2009], are identified in the polar view to vary from latitudes $\lambda_B = -80 \pm 2°$ at $\text{LT}_B = 0100$ to $-75 \pm 5°$ at 0700.

Low-frequency emissions $f \leq f_{ce} + 1$ kHz (red) appear as local sources, widely distributed in all directions in Figure 2a, while strikingly matching the ionospheric footprint of the field lines crossed by Cassini on the polar view (green line). Based on the spacecraft velocity, the dimension of the overall source region along Cassini's trajectory is ~ 51000 km. Events A, B, and C, previously identified as traversed sources, display shorter and similar dimensions of 1800 km for event A, and 900 km for events B and C, corresponding to latitudinal widths of $\sim 0.2°$ and $\sim 0.1°$ respectively, comparable to $\sim 0.2°$ values at Earth (for a typical AKR source at a 3 R_E altitude and a north-south extent of 100 km), but with sources located much farther from the planet. This suggests successive (≥ 3) encounters of SKR curtains, consistent with sub-ovals often observed in UV aurorae [W. Pryor, pers. com.], even if the accuracy of the radio source location was not sufficient to confirm it here.

The unusual distribution of local and distant sources in Figure 2b is confirmed and expanded along an extended time-frequency interval by the radio image of Figure 2c, that

maps SKR intensity onto the polar region. It reveals half of the entire radio auroral oval, with the most intense emissions corresponding to the lowest frequencies within the source region shown by Figures 1a and 2a,b. This distribution also lies along an extended spiral shape, whose latitude, and latitudinal extent, decreases, and broadens, with LT until $\lambda_B = -75 \pm 6°$ at $\text{LT}_B = 1300$.

The crossing of intense SKR sources at low frequencies (high altitudes) located close to midnight, coincided with field lines characterizing a spiral auroral oval, starting from very high latitudes on the nightside, and filling in the dawn sector of the polar cap. This unusual distribution of active magnetic field lines is reminiscent of the well known active UV aurorae, possibly triggered by a solar wind compression [*Bunce et al.*, 2010], and followed by a nightside injection related to plasmoid activity [*Jackman et al.*, 2009].

4. CMI resonance and SKR emission frequency

In regions where f_{pe}/f_{ce} is lower than ~ 0.1 and unstable electron distributions are present, CMI emission can be generated by electrons that fulfill the resonance equation: $f = f_{ce}/\Gamma + k_\| v_\|$, where **k** is the wave vector, **v** the electron velocity, the subscript $\|$ refers to the direction parallel to the magnetic field, and $\Gamma = 1/\sqrt{1 - v^2/c^2}$ is the Lorentz factor [*Wu and Lee*, 1979]. At Earth, AKR being mostly emitted perpendicular to the magnetic field, this equation reduces to $f = f_{ce}/\Gamma$. The CMI emission frequency thus lies below f_{ce}, the difference being directly determined by the kinetic energy of resonant electrons.

Assuming nearly perpendicular emission of SKR, Figure 3 shows that hot electrons are the only reliable candidate for SKR generation. Indeed, their kinetic energy, between 6 and 9 keV, leads to f (red) $\sim 2\%$ below f_{ce} (blue), that match observed f_{cut} (black) during

events A, B and C within error bars. Precisely, the correlation coefficient computed over these 3 events (8 measurements) between f and f_{cut} reaches $c = 0.94$. Warm (and cold) electrons lead to frequencies that cannot be distinguished from f_{ce} ($\Gamma \sim 1$), $i.e.$ inconsistent with the observed f_{cut}.

In the case of non-perpendicular emission of SKR, the resonance frequency is modified by the contribution of $k_\parallel v_\parallel$. Unstable electron distributions, such as loss cone or ring distributions, can drive CMI oblique emission from upgoing electrons. Since radio waves can only be radiated away from the planet, this leads to $k_\parallel v_\parallel \geq 0$, which, in turn, implies CMI frequencies higher than the ones derived for purely perpendicular SKR. More precisely, $k_\parallel = N\omega/c \cos\theta$, with N the index of refraction, θ the angle of emission with respect to the local magnetic field vector, and $v_\parallel = v \cos\alpha$, with α the loss cone angle. Using $\alpha \sim 5°$, $\theta \sim 70°$ (compatible with RPWS measurements), and assuming N $\sim$ 1, we computed the contribution of $k_\parallel v_\parallel$, and therefore CMI emission frequencies for cold, warm and hot electrons. None of these frequencies lie below f_{ce} and thus cannot account for the observed f_{cut}.

In summary, we have shown that the SKR cutoff frequencies observed below f_{ce} can only be explained by a perpendicular SKR emission, excited by the 6 to 9 keV (hot) electrons measured by CAPS. In addition, we note that the shell-like distribution of hot electrons mentioned in section 2 is expected to lead to perpendicular emission [*Ergun et al.*, 2000]. These results are consistent with the terrestrial case.

5. Conclusion

Cassini crossed the first source region of exo-terrestrial radio auroral emissions, evidenced by (i) intense SKR at low frequencies, and (ii) $f_{cut} \leq f_{ce}$.

Among the similarities with AKR at Earth, the SKR source region at Saturn is characterized by $f_{pe}/f_{ce} \leq 0.1$, and upward field-aligned currents, consistent with electrons accelerated toward the planet. Local sources, emitted at frequencies below, or close to, f_{ce}, are detected on field lines crossed by Cassini. The auroral source region is dominated by hot electrons, found to be the only reliable source of energy for CMI resonance, and implying SKR emission perpendicular to the magnetic field.

In contrast to Earth, the SKR sources were detected at much lower frequencies (10 kHz), *i.e.* much higher altitudes (4.1 R_S). The auroral region does not reveal any terrestrial-like cavity, devoid of cold plasma, but appears to be naturally tenuous/magnetized enough to permit CMI driven emission, where unstable electrons are present.

This study revealed intense sources crossed at unusual locations (nightside, very high latitude), and part of an extended spiral radio auroral oval, with high latitude dawnside emission, that suggests enhanced auroral activity. More crossings of the SKR source region, planned at the end of the Cassini mission, are needed to study statistically those characteristics, possibly varying with location and time.

References

Bahnsen, A., et al. (1989), Viking observations at the source region of auroral kilometric radiation, *J. Geophys. Res., 94*, 6643–6654.

Benson, R. F., and W. Calvert (1979), Isis 1 observations at the source of auroral kilometric radiation, *Geophys. Res. Lett., 6*, 479–482.

Bunce, E.J. et al. (2010), Extraordinary FAC signatures in Saturns high-latitude magnetosphere: Analysis of Cassini data during Rev. 89, *J. Geophys. Res.,* submitted.

Cecconi, B., and P. Zarka (2005), Direction finding and antenna calibration through analytical inversion of radio measurements performed using a system of two or three electric dipole antennas on a three-axis stabilized spacecraft, *Rad. Sci. 40*, RS3003.

Cecconi, B., et al. (2009), Goniopolarimetric study of the revolution 29 perikrone using the Cassini Radio and Plasma Wave Science instrument high-frequency radio receiver, *J. Geophys. Res., 114*, A03215.

Ergun, R. E., et al. (2000), Electron-Cyclotron Maser Driven by Charged-Particle Acceleration from Magnetic Field-aligned Electric Fields, *Astrophys. J., 538*, 456–466.

Hilgers, A., et al. (1991), Characteristics of AKR sources - A statistical description, *Geophys. Res. Lett., 18*, 1493–1496.

Hilgers, A., et al. (1992), Measurement of the direction of the AKR electric field inside the sources with the Viking satellite, *J. Geophys. Res., 97*, 8381–8390.

Jackman, C., et al. (2009), On the character and distribution of lower-frequency radio emissions at Saturn and their relationship to substorm-like events, *J. Geophys. Res., , 114*, A08211.

Kurth, W. S. et al. (2009), Auroral Processes, *Saturn from Cassini-Huygens*, 333–374.

Kurth, W. S. et al. (2010), A Close Encounter with a Saturn Kilometric Radiation Source Region, *Geophys. Res. Lett.,* submitted.

Lamy, L., et al. (2008), Saturn kilometric radiation: Average and statistical properties, *J. Geophys. Res., 113*(A12), A07201.

Lamy, L., et al. (2009), An auroral oval at the footprint of Saturn's kilometric radio sources, colocated with the UV aurorae, *J. Geophys. Res., 114*, A10212.

Le Queau, D., and P. Louarn (1989), Analytical study of the relativistic dispersion - Application to the generation of the AKR, *J. Geophys. Res., 94*, 2605–2616.

Louarn, P., et al. (1990), Trapped electrons as a free energy source for the AKR, *J. Geophys. Res., 95*, 5983–5995.

Roux, A., et al. (1993), Auroral kilometric radiation sources - In situ and remote observations from Viking, *J. Geophys. Res., 98*, 11,657–11,670.

Wu, C. S., and L. C. Lee (1979), A theory of the terrestrial kilometric radiation, *Astrophys. J., 230*, 621–626.

Zarka, P. (1998), Auroral radio emissions at the outer planets: Observations and theories, *J. Geophys. Res., 103*, 20,159–20,194.
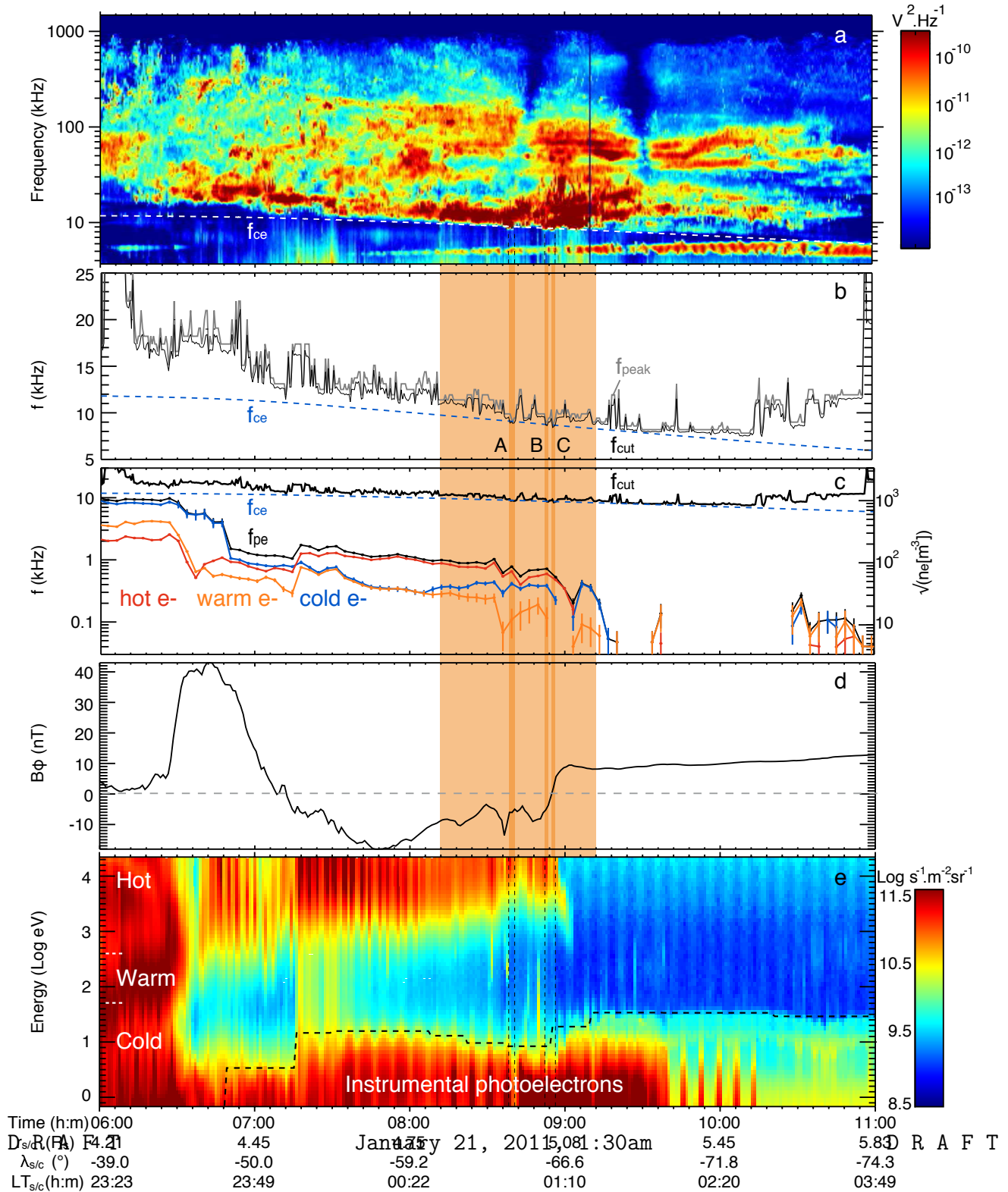
Figure 1. Multi-instrument observations during day 291 of year 2008 over [0600,1100] UT. Panel a displays the RPWS-HFR dynamic spectrum of electric spectral density recorded by the Z monopole (rather than the Stokes parameter S, computed from simultaneous 2-antenna measurements, but noisier at low frequencies). The dashed line indicates the local f_{ce}, as derived from MAG observations. SKR lies between $\sim f_{ce}$ and 1000 kHz. Panel b superimposes f_{peak} (gray) and f_{cut} (black) to f_{ce} (dashed), with a time resolution of 32 s. The typical uncertainty is less than 0.5 % for f_{cut}, and less than 0.05 % (resp. 0.5 %) for f_{ce} after (resp. before) 0821 UT. Orange shaded region maps the interval [0812,0912] UT, where SKR is enhanced below 30 kHz and its low-frequency cutoff reaches f_{ce}. Red shaded events A, B and C mark unambiguous excursions $f_{cut} \leq f_{ce}$. Panel c reproduces f_{cut} and f_{ce} with a log scale, together with the total electron density n_e (expressed in $\sqrt{n_e(cm^{-3})}$, right, and f_{pe}(kHz), left) derived from CAPS-ELS observations (black dots). Colors reveal contributions of cold (blue, ≤ 50 eV), warm (orange, 50-400 eV) and hot (red, ≥ 400 eV) electrons. Panel d shows the azimuthal magnetic field component B_ϕ, measured by MAG with a a 1min resolution and a 0.1nT uncertainty. As a consequence of Maxwell-Ampère equation, its variations indicate field-aligned currents. A positive (negative) slope corresponds to an up-going (down-going) net current. Panel e displays the CAPS-ELS electron spectrogram of differential energy flux (DEF), summed over all anodes at a 3min resolution. Three electron populations are detected: a hot component above 400eV, a cold one below 50eV and a sporadic warm one in between. Cold electrons are partially masked by spacecraft photoelectrons, and all field-aligned down-going electrons were missed due to incomplete pitch angle coverage.
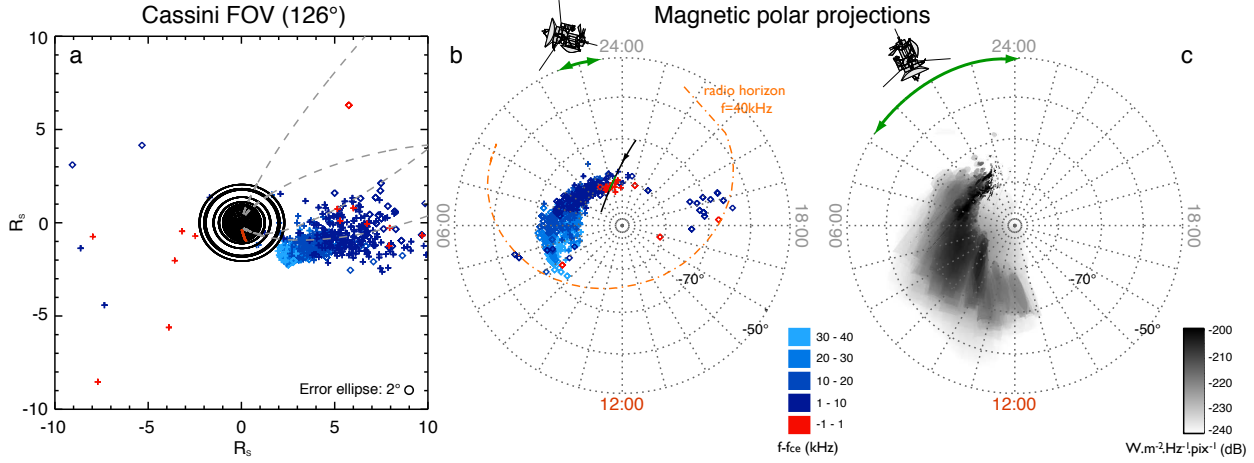
Figure 2. Location of radio sources in Cassini's field of view, or FOV, (panel a) and magnetically projected down to the planet (panel b). The radio data selection is described in the auxiliary material. The time-frequency interval is restricted to [0812,0912] UT (source region) and [7,40kHz] (highest resolution). Crosses (diamonds) refer to directions of arrival that cross (do not cross) their associated isosurface-$f = f_{ce}$ [*Cecconi et al.*, 2009]. Most of the frequencies (plotted in blue scale for increasing ranges of $f - f_{ce}$) correspond to distant sources, clustered along high-latitude magnetic field lines in panel a (dashed, with footprint coordinates LT_B=[0400,0600] and λ_B=[-80°,-75°]), quantitatively identified on the dawnside in panel b. Frequencies plotted in red ($f \leq f_{ce}$+1kHz) reveal local sources, detected through the entire observation plane in panel a, and mapped the ionosphere along field lines crossed by Cassini in panel b, the green (black) line showing the projected spacecraft trajectory for [0812,0912] UT ([0600,1100] UT). Panel c displays the radio map [*Lamy et al.*, 2009] integrated along the extended time interval [0700,1100] UT and frequency range [7,1000kHz]. The global distribution of the footprints of field lines supporting SKR sources follows an unusual spiral shape, starting from narrow very high latitude ∼-80±2° at LT_B=0100, then evolving to broad lower latitudes toward noon until λ_B=-75±6° at LT_B=1300.
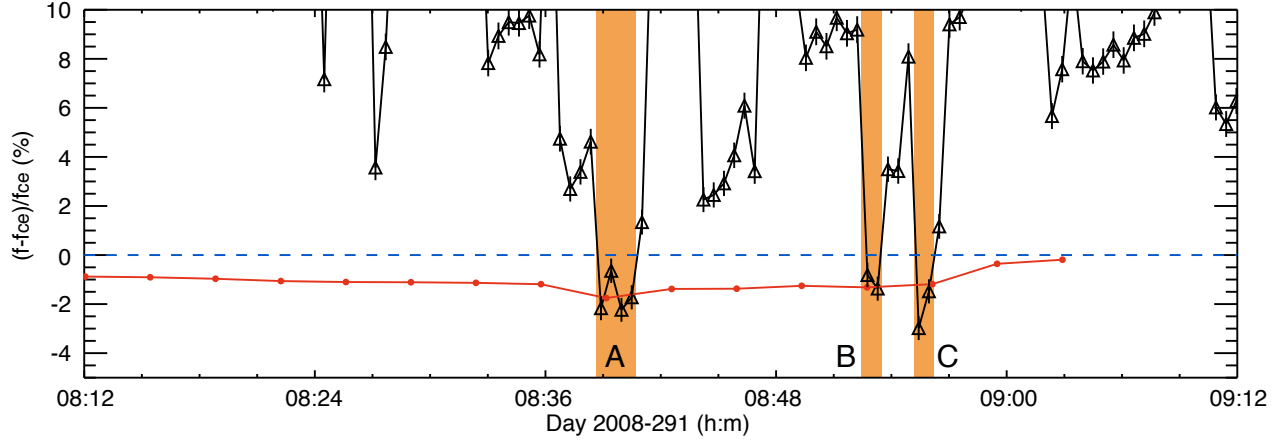
Figure 3. Characteristic frequencies between 0812 and 0912 UT of day 2008-291, expressed relatively to f_{ce}. The SKR cutoff frequency f_{cut}, determined with an accuracy of 0.5 %, is displayed in black, and f_{ce}, in dashed blue. The red curve refers to the CMI resonance frequency f_{ce}/Γ computed with hot electrons observed by CAPS under the assumption of perpendicular SKR emission. The linear correlation coefficient between f and f_{cut}, for the 8 measurements $f_{cut} \leq f_{ce}$ observed during events A, B and C, is $c = 0.96$.